ELSEVIER

Contents lists available at ScienceDirect

Partial Differential Equations in Applied Mathematics

journal homepage: www.elsevier.com/locate/padiff



Approximate solutions to the Gardner equation by spectral modified Exponential Time Differencing method*



Leo Degon, Abhinandan Chowdhury *

Department of Mathematics, Savannah State University, Savannah, GA 31404, USA

ARTICLE INFO

MSC: 15A16 37K10 35Q53

Keywords:
Soliton
Gardner equation
Exponential Time Differencing
Contour integral

ABSTRACT

This manuscript is concerned with the numerical study of spatio-temporal solution profiles of the Gardner equation by implementing a well-known spectral modified numerical scheme based on the Exponential Time Differencing method proposed by Kassam and Trefethan. The modified scheme takes full advantage of contour integral method for improving the numerical stability. But it requires judicious selection of contour path with suitable discretization to minimize the error estimates for solving a particular nonlinear partial differential equation. The efficiency of the scheme is demonstrated by testing it on some test examples – especially measuring discrete maximum norm errors and global relative errors. The associated conservative laws are also numerically verified via attaining very insignificant deviation in the conserved quantities from the initial values even after a large simulation time.

1. Introduction

Wave motion describes a wide range of phenomena across many diverse models. Waves are defined by properties and simplest among them is that they travel. Waves have a temporal dimension and a minimum of one spatial dimension and over time waves propagate a change in the amplitude of the wave's medium. There are two fundamental waves types – traveling waves and plane waves. The former, traveling waves are real valued and they maintain a shape, called a wave profile in general, but experiences translation at a constant wave speed c. On the other hand, Plane waves are complex valued form of traveling waves. They have a few parameters to take into account such as wave number k and angular velocity w. As physical phenomena, waves have Galilean relativity and are invariant to translation in space and time.

In the Nineteenth century, a special kind of waves, known as 'permanent' or 'solitary' waves was discovered. Solitary waves are considered to be special because they can propagate without change on the surface of shallow inviscid fluid layers. Another attractive feature of solitary waves is they retain their shape (or individuality) upon interaction. In a sense, they behave as particles which has earned themselves the name *soliton*, ¹ as in modern physics, a suffix-on is used to indicate the particle property. This occurred in the 1970's as studies into quasi-particles gained traction. Nowadays, soliton phenomena are discovered in virtually every discipline of natural sciences, such as nonlinear optics, plasmas, fluid mechanics, electro-magnetic and condensed matter. ^{2,3}

One of the key physical properties of the nonlinear equations which admit soliton solutions is that they have infinite numbers of conservation laws and associated symmetries which are strongly related to their integrability. For example, there exists an infinite sequence of conserved quantities in the KdV equation. Gardner equation, also known as the extended KdV equation, was originally discovered as an auxiliary mathematical tool while deriving the infinite set of local conservation laws of the KdV equation. Later it turned out to be a

E-mail address: chowdhury@savannahstate.edu (A. Chowdhury).

https://doi.org/10.1016/j.padiff.2022.100310

Received 27 November 2021; Received in revised form 1 February 2022; Accepted 20 February 2022

Waves do not necessarily maintain form indefinitely. Two properties that can factor into this are dispersion and dissipation. Solitons have the ability to travel long distances without collapsing or spreading out. Normal waves usually collapse or spread out because they have different speeds and indexes of refraction depending on their frequency and a wave can be thought of as a superposition of different frequency waves. This tendency for the wave profile to spread out is referred to as dispersion and is modeled by a u_{xxx} term. On the other hand, dissipation is based on a u_{xx} term and models the loss of the waves amplitude and energy. However, the governing equations for solitons are, as a rule, nonlinear. Due to the effect of nonlinearity, the wave steepens and then, if further continued, it will break. Now since dispersion causes the opposite effect of steepening, these two effects provide the equilibrium to produce a permanent shape. In this way, dispersion (or dissipation) plays an essential role in generating solitons by engaging in a balancing act with the nonlinearity. One fundamental equation which describes the propagation of nonlinear waves in one-dimensional case in a weakly dispersive medium is the famous Korteweg-de Vries (KdV) equation.⁴

^{*} Corresponding author.

fundamental mathematical model for the description of weakly nonlinear dispersive waves, but in the presence of higher order nonlinearity effects (described by the cubic term). It appears in the following form:

$$u_t + \mu_1 u u_x + \mu_2 u^2 u_x + \mu_3 u_{xxx} = 0, (1.1)$$

where, u=u(x,t) and μ_1 , μ_2 and μ_3 are constants. It has two nonlinear terms in the quadratic $\left((u^2)_x\right)$ and cubic $\left((u^3)_x\right)$ forms and the dispersive term is of third order (u_{xxx}) . It should be noted that the Gardner equation could be derived while searching for a new soliton hierarchy as well. One such funding is recently reported in Ref. 6 where a novel counterpart of well-known Boiti-Pempinelli-Tu soliton hierarchy is presented which helps us derive the Gardner equation.

The Gardner equation has been used to model rogue waves in layered fluids, such as in atmosphere and river mouths, including both solitons and undular bore solutions.⁷ One of the best known applications of this equation is modeling of large-amplitude internal waves.^{8,9} The Gardner Equation is not limited to water alone. Its applicability can be found in diverse situations in plasma physics. Another significant feature of Gardner equation is its ability to describe the propagation of negative ion acoustic plasma waves, ^{10,11} a phenomenon found in planetary magnetospheres and in the mesosphere. The Gardner equation is also used to study various dynamics of positron-acoustic solitons which helps understanding auroral acceleration, supernova, pulsars environments, cluster explosions, and active galactic nuclei, etc.¹² Apart from describing its significance amid numerous interesting physics phenomena, the Gardner equation is also being rigorously investigated to generate many other families of periodic and localized solitary wave solutions e.g., by performing the bifurcation theory of dynamical systems¹³ to Eq. (1.1).

This paper is an effort to employ a spectral modified exponential time differencing (ETD) method (presented by Kassam and Trefethan¹⁴) to study the numerical solutions to the Gardner equations. Over the years various types of ETD Runge–Kutta (ETDRK) methods for solving nonlinear problems have been proposed and studied. Among them, the fourth order ETD method proposed by Cox and Matthews¹⁵ is worth mentioning in which, new Runge–Kutta versions of ETD schemes were introduced to obtain higher order accuracy. This method is known as *Exponential Time Differencing fourth-order Runge–Kutta* (ETDRK4). But it suffers from numerical instability which was explored in Ref. 14. This paper¹⁴ also includes a modified version of ETDRK4 capable of evaluating computationally sensitive expressions with high accuracy. Therefore, the modified version (also popular as mETDRK4) can be considered to be an improvement upon ETDRK4 method. Arguably mETDRK4 is the first fully practical ETD method for general use.

2. ETDRK schemes

2.1. ETDRK4 scheme

In this section, first we will briefly introduce the ETD method, then introduce the ETDRK4 and mETDRK4 methods. To demonstrate that, let us consider a general first order ODE:

$$\frac{du}{dt} = cu + f(u, t),\tag{2.1}$$

where c is constant and f represents the nonlinear terms. We can recast Eq. (2.1) in the form $\dot{u} = L(u) + N(u)$, where L and N are linear and nonlinear functions, respectively. Rearranging the terms of (2.1), i.e., moving the linear term to the left side, and multiplying both sides of (2.1) by the integrating factor of e^{-ct} , (2.1) can be rewritten as:

$$\frac{d}{dt}\left(e^{-ct}u\right) = e^{-ct}f.$$

Now, step by step, first integrating both sides over the interval from $t = t_n$ to $t = t_n + h = t_{n+1}$, then by allowing a change of variable for t, namely $\tau = t - t_n$ allows us to recast the scheme as:

$$u_{n+1} = e^{ch} u_n + e^{c(t_n + h)} \int_0^h e^{-c\tau} f(u(\tau + t_n), \tau + t_n) d\tau.$$
 (2.2)

Eq. (2.2) can be further generalized by expressing it as a system of ODEs:

$$u_t = \mathbf{L}u + \mathbf{N}(u, t),\tag{2.3}$$

where L and N are linear and nonlinear discretization operators, respectively. At this point, based on the method of approximating the integral in the R.H.S. of (2.2), different ETD schemes can be derived. Provided below the formulae of the fourth order scheme of this type based on Runge–Kutta time stepping as introduced in Ref. 15. In this paper it was argued that the derivation of this scheme requires a symbolic manipulation system as they are not obvious.

$$\begin{split} &a_n = e^{\mathbf{L}h/2}u_n + \mathbf{L}^{-1}(e^{\mathbf{L}h/2} - \mathbf{I})\mathbf{N}(u_n, t_n) \\ &b_n = e^{\mathbf{L}h/2}u_n + \mathbf{L}^{-1}(e^{\mathbf{L}h/2} - \mathbf{I})\mathbf{N}(a_n, t_n + h/2) \\ &c_n = e^{\mathbf{L}h/2}a_n + \mathbf{L}^{-1}(e^{\mathbf{L}h/2} - \mathbf{I})\big(2\mathbf{N}(b_n, t_n + h/2) - \mathbf{N}(u_n, t_n)\big) \\ &u_{n+1} = e^{\mathbf{L}h}u_n + h^{-2}\mathbf{L}^{-3}\Big\{ \left[-4 - \mathbf{L}h + e^{\mathbf{L}h}(4 - 3\mathbf{L}h + (\mathbf{L}h)^2) \right]\mathbf{N}(u_n, t_n) \\ &+ 2 \left[2 + \mathbf{L}h + e^{\mathbf{L}h}(-2 + \mathbf{L}h) \right] \big(\mathbf{N}(a_n, t_n + h/2) + \mathbf{N}(b_n, t_n + h/2) \big) \\ &+ \left[-4 - 3\mathbf{L}h - (\mathbf{L}h)^2 + e^{\mathbf{L}h}(4 - \mathbf{L}h) \right]\mathbf{N}(c_n, t_n + h) \Big\} \end{split}$$

In this updated formula for ETDRK4, if we separately treat the expressions in square brackets as coefficients, we can write

$$Q = \mathbf{L}^{-1} \left(e^{\mathbf{L}h/2} - 1 \right)$$

$$\alpha = h^{-2} \mathbf{L}^{-3} \left[-4 - \mathbf{L}h + e^{\mathbf{L}h} (4 - 3\mathbf{L}h + (\mathbf{L}h)^{2}) \right]$$

$$\beta = h^{-2} \mathbf{L}^{-3} \left[2 + \mathbf{L}h + e^{\mathbf{L}h} (-2 + \mathbf{L}h) \right]$$

$$\gamma = h^{-2} \mathbf{L}^{-3} \left[-4 - 3\mathbf{L}h - (\mathbf{L}h)^{2} + e^{\mathbf{L}h} (4 - \mathbf{L}h) \right].$$
(2.4)

These coefficients are higher order analogues of g(z), defined as $(e^z - 1)/z$. Accurate computation of this function poses a formidable problem which is well documented in the literature of numerical analysis. This problem is particularly discussed by Higham¹⁶ and Friesner et al.¹⁷ in their monographs.

The equations in (2.4) suffer from catastrophic cancellation if implemented directly in this format. In fact, the last three equations have expressions similar to the form which causes rounding errors rapidly.

2.2. mETDRK4 method

In order to efficiently implement the ETDRK4 scheme in general, Kassam and Trefethen proposed to evaluate these expressions with high accuracy by using an approximation based on contour integration from complex analysis. More specifically, using the Cauchy integral representation on a circle with radius 1 centered at z for $|z| < z_0$, we have

$$\phi_l(z) = \frac{1}{2\pi i} \int_{\Gamma} \frac{\phi_l(s)}{s-z} \mathrm{d}s \quad \text{where} \quad \phi_l(z) = \sum_{k=l}^{\infty} \frac{1}{k!} z^{k-l} = \sum_{k=0}^{\infty} \frac{1}{(k+l)!} z^k$$

Note that, from the above expression, if we write $\phi_l(z)$ as $\frac{1}{z^n}\left(e^z-\sum_{k=0}^{l-1}\frac{z^k}{k!}\right)$, it actually allows us to attain first l ' ϕ ' functions involved in an ETD method of order l. First few values are as follows:

$$\phi_1(z) = (e^z - 1)/z, \quad \phi_2(z) = (e^z - z - 1)/z^2,$$

$$\phi_3(z) = (e^z - z^2/2 - z - 1)/z^3, \dots$$

As l increases, these functions become increasingly difficult to evaluate for small z, mainly due to the subtraction error. For scalar case, one can use the explicit formula and truncated Taylor series for large and small z, respectively. But when z is a matrix, numerical instability occurs because usually z has large, and more critically, very small (zero or close to zero) eigenvalues.

The Cauchy integral formula in matrix form appears as:

$$\phi_l(z) = \frac{1}{2\pi i} \int_{\Gamma} \phi_l(s) (s\mathbf{I} - z)^{-1} ds,$$

where the contour Γ encloses all the eigenvalues of z. The integral can be approximated by using the *periodic trapezium* rule which is known to be a spectral method in this case. The approximations can be carried out by considering a circle of M points $z_k = e^{2\pi i k/M}$:

$$\phi_l(z) \approx \frac{1}{M} \sum_{k=1}^{M} \phi_l \left(z + e^{2\pi i k/M} \right), \quad l \ge 0.$$
 (2.5)

When **L** is real, we can select our contour Γ to be a circle of radius R. We integrate over the upper-half of the complex plane and take the real part of the result. By discretizing the contour path with the points

$$t_k = R \exp(i(k - k_0)\pi/M)$$
 for $k = 1, 2, 3, ... M$, (2.6)

a contour integral

$$\phi_l(h\mathbf{L}) = \frac{1}{2\pi i} \int_{\Gamma} \phi_l(s)(s\mathbf{I} - h\mathbf{L})^{-1} ds,$$

can be approximated as

$$\phi_l(h\mathbf{L}) = \frac{1}{M} \mathcal{R} \sum_{k=1}^M t_k \phi_l(t_k) (t_k \mathbf{I} - h\mathbf{L})^{-1}.$$

Though the approximation in Eq. (2.5) was originally designed for scalar or diagonal matrices, a general form of Eq. (2.5) intended for non-diagonal cases is proposed in Ref. 14. This approximation remedies the numerical instability to a reasonable extent! The functions in Eqs. (2.4) can now be computed by using Eq. (2.5). For example, Q can be approximated as follow: let q = Lh and the function Q becomes

$$\begin{split} Q &= \mathbf{L}^{-1} \left(e^{\mathbf{L}h/2} - 1 \right) = h \frac{e^{q/2} - 1}{q} = \frac{h}{M} \sum_{k=1}^{M} \frac{e^{(q+z_k)/2} - 1}{q + z_k} \\ &= \frac{h}{M} \sum_{k=1}^{M} \frac{e^{(\mathbf{L}h + z_k)/2} - 1}{\mathbf{L}h + z_k}, \end{split}$$

where $z_k = e^{2\pi i k/M}$ denote the roots of unity.

Upon evaluating the functions Q, α , β and γ which heavily involve the linear operator as shown in (2.3), we have the choice to evaluate the nonlinear term spectrally or pseudo-spectrally while carrying out the Runge-Kutta time-stepping scheme. As we know, the Gardner equation has two nonlinear terms: uu_x and u^2u_x . The term uu_x can be evaluated spectrally by recasting it as $(1/2)(u^2)_x$. Similarly, u^2u_x can be written as $(1/3)(u^3)_x$. For the present work, we have evaluated both terms spectrally though the cubic term poses the relatively severe case of nonlinearity. For complicated nonlinear term (e.g., u^2u_x) one can apply the pseudo-spectral approximation in the following manner: first evaluate $u_x = \mathcal{R} \left[\mathcal{F}^{-1}(ik\hat{u}) \right]$ where $\hat{u} = \mathcal{F}(u)$ – the Fourier transform of u; then, u^2u_x can be approximated by multiplying $\mathcal{R}\left[\mathcal{F}^{-1}(ik\hat{u})\right]$ by u^2 . Though pseudospectral approach performs better while evaluating complicated nonlinear terms, for many cases, using this approach requires setting up substantially small time steps, thus increasing the overall computational time of the method.

3. Numerical simulations and discussions

In this section, we present the results of numerical experiments carried out by implementing the mETDRK4 scheme on three test problems in order to demonstrate the efficiency and accuracy of the scheme. Similar test problems are numerically studied in Ref. 18 where a collocation method based on exponential B-spline is successfully applied. All the numerical experiments are conducted in MATLAB 9.3 platforms. In order to determine the accuracy of the schemes, we have measured the discretized maximum norm errors L_{∞} and global relative error (GRE) defined as:

$$L_{\infty} = \max_{i} |e_{i}|, \quad GRE = \frac{\sum_{i} |e_{i}|}{\sum_{i} |u_{i}|},$$

where $e_i = u_i - U_i$, $u_i = u(x_i, t)$, and $U_i = U(x_i, t)$ are the ith exact and numerical solutions, respectively. The summation is taken over all grid points together.

The conservation laws also validate the accuracy of the proposed algorithm. These laws describe the conservation of fundamental physical quantities. The associated conserved quantities are expected to keep their initial values as time proceeds. ¹⁹ Numerical investigation of associated conserved quantities provides a rigorous validation of the efficacy of the numerical scheme especially in the case of nonavailability of the analytical solutions. The lowest three conservation laws are

$$M = \int_{-\infty}^{\infty} u dx, \quad E = \int_{-\infty}^{\infty} u^2 dx, \quad H = \int_{-\infty}^{\infty} \left(\alpha_1 u^3 + \alpha_2 u^4 + \alpha_3 (u_x)^2 \right) dx$$

which correspond to conservation of linear momentum, energy and the Hamiltonian, respectively. The conserved quantities can be measured by evaluating the integrals albeit for a finite computational domain – which is done by employing the trapezoidal numerical integration method with the aid of a built-in MATLAB function, trapz. To find the constants α_1 , α_2 , and α_3 , we have used the concept of *Fréchet derivative* which is also known as the variational derivative.²⁰ The Fréchet derivative, $\delta F/\delta u$, of the operator $F\{u\}$, is defined by

$$\int_{-\infty}^{\infty} v \frac{\delta F}{\delta u} dx = \lim_{\epsilon \to 0} \frac{\partial}{\partial \epsilon} \int_{-\infty}^{\infty} F(u + \epsilon v) dx$$

for all continuous v. Then it can be shown that, if $F(u)=f(u,u_x,u_{xx},\dots)$, then $\delta F/\delta u$ corresponds to the Euler–Lagrange operator, i.e.,

$$\frac{\delta F}{\delta u} = \frac{\partial f}{\partial u} - \frac{\mathrm{d}}{\mathrm{d}x} \frac{\partial f}{\partial u_x} + \frac{\mathrm{d}^2}{\mathrm{d}x^2} \frac{\partial f}{\partial u_{xx}} \cdots$$
 (3.1)

F(u) can be selected in such a way that upon applying the R.H.S. expression from Eq. (3.1), we can exactly attain the terms in the R.H.S of the Eq. (1.1), re-written by keeping only the u_t term in the L.H.S. and moving every other terms to the R.H.S. F(u) will provide the integrand in the expression of the Hamiltonian.

In order to measure the absolute relative changes of these quantities at any time t>0, $C(M_t)$, $C(E_t)$, and $C(H_t)$ are defined as

$$C(M_t) = \left| \frac{M_t - M_0}{M_0} \right|, \quad C(E_t) = \left| \frac{E_t - E_0}{E_0} \right|, \quad C(H_t) = \left| \frac{H_t - H_0}{H_0} \right|,$$

where M_0 , E_0 and H_0 are initial, M_t , E_t and H_t are the quantities at the time t > 0.

3.1. Test example 01

In this example, we use the Gardner equation with the parameters chosen as $\mu_1 = 4$, $\mu_2 = -3$ and $\mu_3 = 1$ for Eq. (1.1) which gives:

$$u_t + 4uu_x - 3u^2u_x + u_{xxx} = 0, (3.2)$$

It admits an exact solution:

$$u_e(x,t) = \frac{2}{12 + 3\sqrt{14}\cosh\left[\frac{(-x+5)}{3} + \frac{t}{27}\right]},$$

which also allows us to avail the initial data $u_0(x) = u(x, t = 0)$. The Gardner equation produces a single solitary wave with this form. The solution in fact represents the propagation of an initial positive pulse as demonstrated in Fig. 1 in the time domain [0, 20]. In Fig. 2, we have shown the absolute error profile in the same time domain. It can be noticed that the maximum error stays well within the range of 10^{-2} even for such a large time domain. The computational region is fixed on I = [-20, 30] and the time step size (Δt) and the spatial step size (Δt) both are set as 0.1.

The discretized maximum norm errors L_∞ and GREs at some distinct times are reported in Table 1 for the test example 01. Table 1 also includes the values of conserved quantities at distinct times. It can be observed that values are being preserved as time progresses which indicates towards a stable numerical scheme. To quantify the deviations of the conserved quantities from their initial values, we have measured

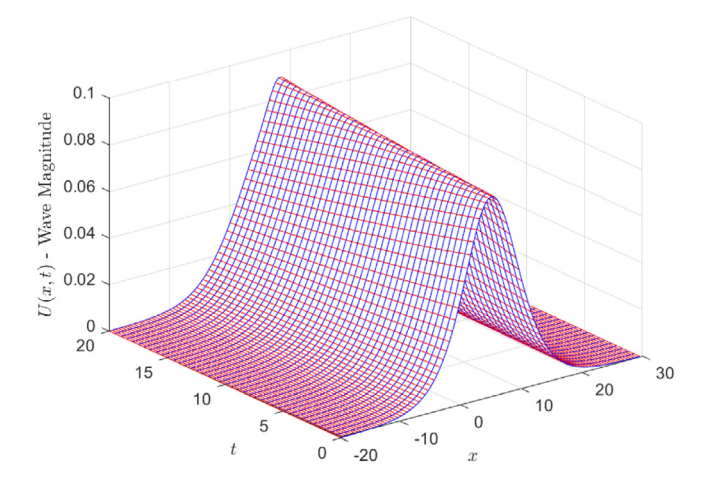


Fig. 1. Wave propagation of initial positive pulse for Test Example 01.

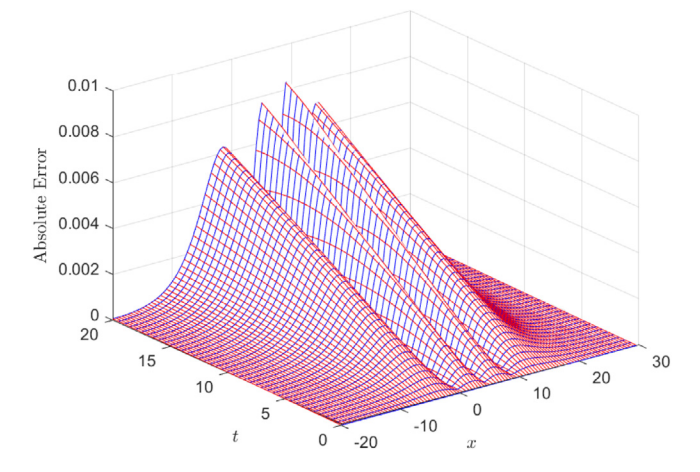


Fig. 2. Absolute error profile for the numerical approximation from Test Example 01.

the absolute relative changes (i.e., $C(M_t)$, $C(E_t)$, and $C(H_t)$) of these quantities at some distinct time T>0 which are reported in Table 2. In the case of linear momentum and energy, they are preserved up to at least 4 decimal places even for T=20.0. For the Hamiltonian, the change can be noticed only from the 5th decimal digit until T=10.0. All calculations are carried out by using the similar computational region as well as the same time and spatial step size as noted in the previous paragraph.

Also, for finding the α_1 , α_2 , and α_3 in the integral of the Hamiltonian for the Test Example 01, we have used the relation (3.1). If we select

$$F(u) = f(u, u_x, u_{xx}, \dots) = -\frac{2}{3}u^3 + \frac{1}{4}u^4 + \frac{1}{2}(u_x)^2,$$

it can be easily verified that the *Hamiltonian* formulation of the Eq. (3.2) will be

$$\frac{\partial u}{\partial t} = \frac{\partial}{\partial x} \left\{ \frac{\delta}{\delta u} \left(-\frac{2}{3} u^3 + \frac{1}{4} u^4 + \frac{1}{2} (u_x)^2 \right) \right\}.$$

3.2. Test example 02

The second version of the Gardner equation (Eq. (3.3)) that we modeled using this method yields kink type soliton solutions. The kink soliton is topological which implies that the boundary conditions at infinity for the wave are topologically different to the vacuum it is in Ref. 21. These kink solitons are typically characterized by their permanent profiles, which means they are time-independent. A good

Table 1 GREs, L_{∞} , and conserved quantities for $\Delta t = 0.1$, $x \in [-20, 30]$ and $\Delta x = 0.1$ for Test example 01.

T	GRE	L_{∞}	Momentum	Energy	Hamiltonian
0.1	6.8607E-04	3.9238E-05	1.044586714	6.0134543E-02	4.0653191E-03
0.2	1.3698E-03	7.8594E-05	1.044586592	6.0134555E-02	4.0653093E-03
0.5	3.4191E-03	1.9644E-04	1.044586380	6.0134591E-02	4.0652353E-03
1.0	6.8338E-03	3.9367E-04	1.044586162	6.0134651E-02	4.0649633E-03
2.0	1.3661E-02	7.9043E-04	1.044585894	6.0134772E-02	4.0638612E-03
5.0	3.4138E-02	1.9992E-03	1.044585455	6.0135124E-02	4.0560559E-03
10.0	6.8243E-02	4.0891E-03	1.044585000	6.0135644E-02	4.0275851E-03
15.0	1.0232E-01	6.2571E-03	1.044584742	6.0135996E-02	3.9067078E-03

Table 2 Absolute relative changes of conserved quantities at different time T for $\Delta t = 0.1$, $x \in [-20, 30]$ and $\Delta x = 0.1$ for Test example 01.

T	M_0	E_0	H_0	$C(M_T)$	$C(E_T)$	$C(H_T)$
1.0	1.044587	6.01345E-02	4.06532E-03	8.673E-07	2.009E-06	8.808E-05
5.0	1.044587	6.01345E-02	4.06532E-03	1.544E-06	9.870E-06	2.279E-03
10.0	1.044587	6.01345E-02	4.06532E-03	1.980E-06	1.852E-05	9.282E-03
15.0	1.044587	6.01345E-02	4.06532E-03	2.227E-06	2.436E-05	2.137E-02
20.0	1.044587	6.01345E-02	4.06532E-03	2.384E-06	2.521E-05	3.902E-02

real-world example of a kink solution is a Bloch wall between two magnetic domains in a ferromagnet. The parameters are chosen as $\mu_1 = 1$, $\mu_2 = -5$ and $\mu_3 = 1$ which yields

$$u_t + uu_x - 5u^2u_x + u_{xxx} = 0. (3.3)$$

This equation has an exact solution:

$$u_e(x,t) = \frac{1}{10} \left(1 - \tanh \left(\frac{\sqrt{30}}{60} \left(x - \frac{t}{30} \right) \right) \right),$$

which allows us to derive the initial condition $u_0(x) = u(x, t = 0)$. The mETDRK4 algorithm is applied to find the numerical solutions to Eq. (3.3). Similar to the Test Example 01, the discretized maximum norm errors L_{∞} and GREs at some distinct times are measured and reported in Table 3. The scheme is allowed to run up to the final time t = 20 in the finite interval [-80, 80]. The kink wave profile and the absolute error profile are shown in Fig. 3 and Fig. 4, respectively. The time step size (Δt) and the spatial step size (Δx) both are fixed as 0.1. From Fig. 4, it is obvious that maximum error stays well within the range of 10^{-3} even for (t = 20). Also the error is larger around x = 0 which is expected from kink-shape wave. We have also tabulated absolute relative changes in the conserved quantities at some distinct time T > 0 in Table 4. The magnitude of changes in all three conserved quantities for Test Example 02 remain essentially in the same range as that observed for Test Example 01. It is obvious that all three conserved quantities remain unchanged up to at least four decimal digits for various simulation time.

3.3. Test example 03

Next, we study the conservation of the linear momentum, energy and the Hamiltonian for the following form of the Gardner equation

$$u_t + 6uu_x + 6u^2u_x + u_{xxx} = 0, (3.4)$$

by using the *Gaussian initial condition*, $u(x,0) = e^{-x^2}$. Table 5 depicts the measurement of three conserved quantities over the interval [-80, 80] until the final time T = 20. In can be observed that conservation is good throughout the simulation. The conservation of momentum is preserved up to 4 decimal places until large simulation time T = 10. Similarly, the magnitude of deviation for energy is measured beyond 10^{-2} only after T = 10. Though for the Hamiltonian, similar magnitude of deviation in the conserved quantity occurs around T = 5.

We conclude this section by noting an important observation regarding the choice of contour Γ . It was clearly stated in the paper

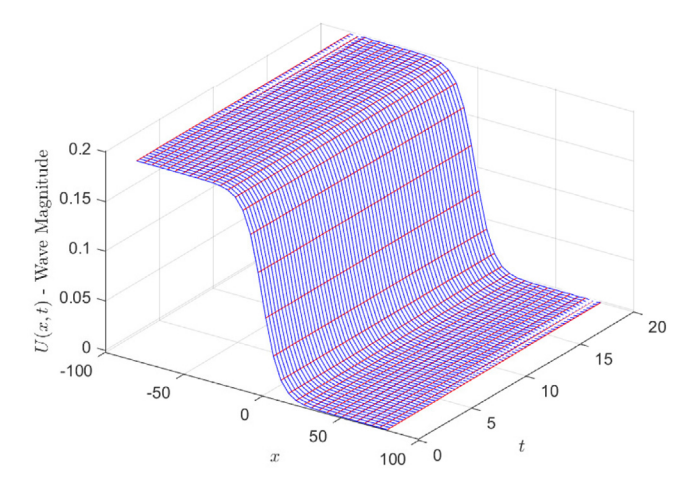


Fig. 3. Propagation of Kink type wave for Test Example 02.

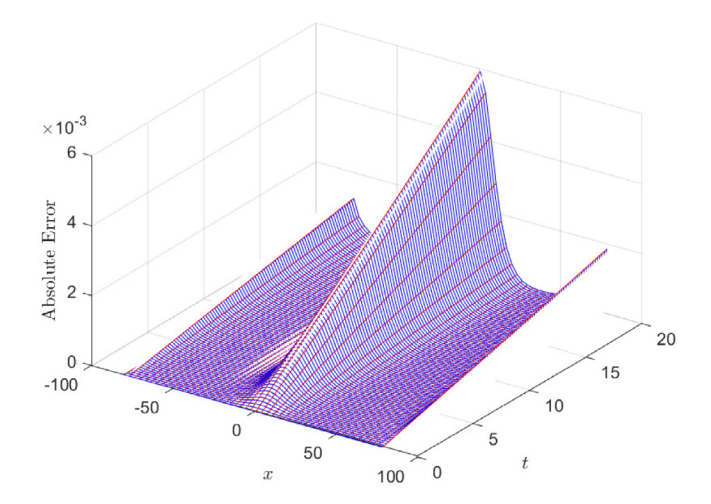


Fig. 4. Absolute error profile for the numerical approximation from Test Example 02.

Table 3 GREs, L_{∞} and conserved quantities for $\Delta t=0.1,\ x\in[-80,80]$ and $\Delta x=0.1$ for Test example 02.

Time	GRE	L_{∞}	Momentum	Energy	Hamiltonian
0.1	5.1442E-05	2.9570E-05	15.99999987	2.9809121	1.0897243E-01
0.2	1.0288E-04	5.9142E-05	15.99999973	2.9809129	1.0897331E-01
0.5	2.5720E-04	1.4786E-04	15.99999933	2.9809156	1.0897603E-01
1.0	5.1438E-04	2.9575E-04	15.99999865	2.9809201	1.0898094E-01
2.0	1.0287E-03	5.9159E-04	15.99999725	2.9809291	1.0899217E-01
5.0	2.5709E-03	1.4796E-03	15.99999283	2.9809569	1.0903716E-01
10.0	5.1393E-03	2.9610E-03	15.99998466	2.9810057	1.0915006E-01
15.0	7.7049E-03	4.4434E-03	15.99997554	2.9810575	1.0931084E-01

Table 4 Absolute relative changes of conserved quantities at different time T for $\Delta t = 0.1$, $x \in [-80, 80]$ and $\Delta x = 0.1$ for Test example 02.

T	M_0	E_0	H_0	$C(M_T)$	$C(E_T)$	$C(H_T)$
1.0	16.0	2.9809112	1.08972E-01	8.438E-08	2.989E-06	8.583E-05
5.0	16.0	2.9809112	1.08972E-01	4.481E-07	1.535E-05	6.018E-04
10.0	16.0	2.9809112	1.08972E-01	9.588E-07	3.172E-05	1.638E-03
15.0	16.0	2.9809112	1.08972E-01	1.529E-06	4.910E-05	3.113E-03
20.0	16.0	2.9809112	1.08972E-01	2.155E-06	6.745E-05	5.035E-03

by Kassam and Trefethen¹⁴ that selection of contour depends on the problem under consideration. According to,¹⁴ one must ensure that the eigenvalues are enclosed by the contour and it can be achieved through different choices. In their paper, they suggested to take Γ to be a circle

Table 5 Conserved quantities for $\Delta t = 0.1$, $x \in [-80, 80]$ and $\Delta x = 0.1$ for Test example 03.

Time	Momentum	Energy	Hamiltonian
0.0	1.691436609	0.8756760777	21.19962092
0.1	1.691436608	0.8756804146	21.19977423
0.2	1.691436602	0.8756821104	21.19986803
0.5	1.691436548	0.8756713664	21.1997926
1.0	1.69143634	0.8756009404	21.19848036
2.0	1.691435482	0.8752672486	21.19145343
5.0	1.691429424	0.8729142508	21.13733488
10.0	1.691408465	0.8670010451	20.96581856
15.0	1.69137624	0.8652143387	20.76894611
20.0	1.691336595	0.8751498617	20.63601928

and to discretize the contour path with M (preferably 32 or 64) equally spaced points

$$t_k = 1.0 \exp(i(k - 0.5)\pi/M)$$
, for $k = 1, 2, ..., M$

before approximating the contour integral.

What we have found is that the choice of the value $k_0=0.5$ (Fig. 5) is not optimum. Changing this value makes the upper half of the circle rotate. For example, in Fig. 6 where $k_0=2.5$, we can observe that the leftmost point which was above the positive real axis for $k_0=0.5$, now goes below it, thus possibly enclosing more eigenvalues situated at the shaded region and consequently improving the error estimates.

In this context, one numerical approach introduced by Schmelzer 22 is worth mentioning. Schemlzer made the existing approach more efficient by using the complex contour approach only for values of z close to the pole, e.g., |z| < 1/2. This requires a special care when devising an algorithm to compute the contour integrals while employing different approach to the values of z based on their proximity to the pole. We wish to address this issue in detail elsewhere.

4. Conclusion

The Fourier spectral modified ETD method with Runge-Kutta time marching (mETDRK4) is implemented to solve the Gardner equations a nonlinear PDE from the KdV family which consists of two nonlinear terms. The scheme introduces a novel concept of using contour integral method to evaluate terms usually prone to numerical instability when eigenvalues are close to zero. Though current problem poses the challenge of severe nonlinearity, the differentiation is carried out spectrally in order to avoid using very small time step size. The performance and applicability of the scheme have been investigated by testing it on several test problems - especially evaluating the discretized maximum norm errors and global relative errors. The first Gardner equation yields single solitary wave and the second one yields kink-type soliton solutions. Another version of the Gardner equation with Gaussian initial condition is also numerically studied. The computed numerical solutions maintain good accuracy compared with the respective exact solutions. The conserved quantities are also evaluated along with their absolute relative changes to observe the validity and accuracy of the scheme even when there exists no exact solution. It is also argued that rearranging the contour points which discretize the contour path could be effective to improve the accuracy of the numerical approximations.

It must be noted that the mETDRK4 scheme is not completely free of limitations. It suffers from limitations such as (a) it is fairly slow – need M matrix inverses; (b) one needs to know where eigenvalues are; and (c) inaccurate if contour too large: error $\propto R^M/M!$. Despite these drawbacks, it has been quite popular since its inception because it allows a control of the accuracy in evaluating functions (ϕ_l) prone to numerical instabilities. In fact, it is sufficient to use a small number of Fourier modes in the numerical evaluation of the complex contour integral in order to attain machine accuracy while determining ϕ_l functions. Building on this work, more improved exponential integrators are derived for solving stiff PDEs. Since exponential integrators require the

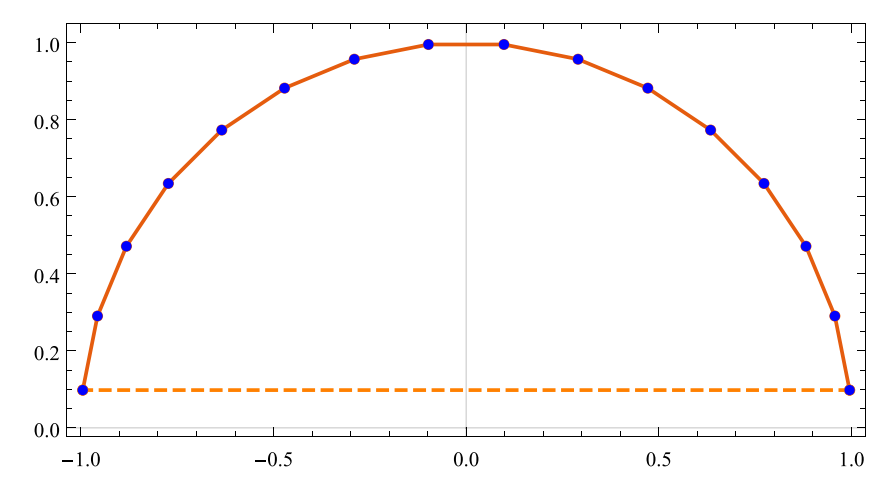


Fig. 5. Contour Region by setting $k_0 = 0.5$ according to Eq. (2.6).

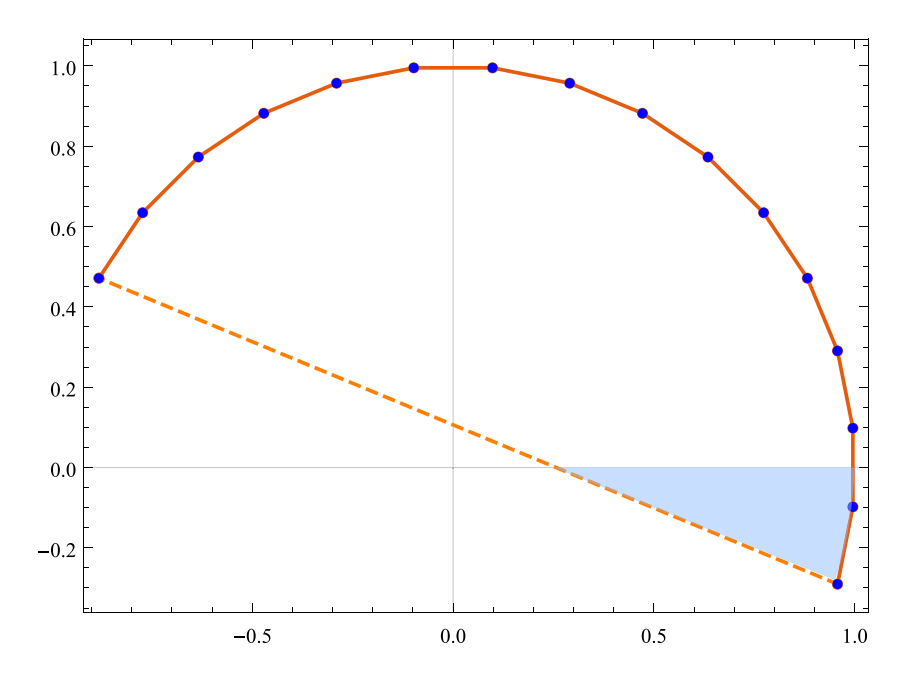


Fig. 6. Contour Region by setting $k_0 = 2.5$ according to Eq. (2.6).

evaluation of f(A) where A is a negative semidefinite matrix and f is an exponential function or ϕ_l -type functions, more efforts were made in devising schemes to better tackle the issue of numerical approximation of ϕ_l functions. Many novel approaches were introduced in this context which includes using uniform rational Chebyshev approximations, scaling and squaring or the application of the Trapezoid rule on Talbottype contours. ²³ It is also shown that the computation of these functions does not require significant amount of additional time while extended to the problems with higher spatial dimension. Application of these schemes for (2+1)-dimensional Gardner or other KdV-type equations is yet under investigation, and will be the subject of future research.

Declaration of competing interest

The authors declare that they have no known competing financial interests or personal relationships that could have appeared to influence the work reported in this paper.

Acknowledgments

The authors are grateful to anonymous referees for their valuable comments and suggestions which improved the quality of this

manuscript. The authors also gratefully acknowledge supports from the US Department of Education under PR/Award number P382G170103 and the US National Science Foundation under grant number 1800798.

References

- 1. Herman R. Solitary waves. Am Sci. 1992;80(4):350-361.
- Ablowitz MA, Segur H. Solitons and the Inverse Scattering Transform. Philadelphia, PA: Society for Industrial and Applied Mathematics; 1981.
- Taha TR, Ablowitz MI. Analytical and numerical aspects of certain nonlinear evolution equations. II. Numerical, nonlinear Schrödinger equation. *J Comput Phys.* 1984;55(2):203–230. http://dx.doi.org/10.1016/0021-9991(84)90003-2.
- Korteweg DJ, de Vries G. XLI. On the change of form of long waves advancing in a rectangular canal, and on a new type of long stationary waves. *Lond, Edinb, Dublin Philos Mag J Sci.* 1895;39(240):422–443. http://dx.doi.org/10.1080/ 14786449508620739.
- Miura RM, Gardner CS, Kruskal MD. Korteweg-de vries equation and generalizations. II. Existence of conservation laws and constants of motion. *J Math Phys.* 1968;9(8):1204–1209. http://dx.doi.org/10.1063/1.1664701.
- Appiah EA, Manukure S. An integrable soliton hierarchy associated with the Boiti–Pempinelli–Tu spectral problem. *Modern Phys Lett B*. 2021;35(17):2150282. http://dx.doi.org/10.1142/S0217984921502821.
- Kamchatnov AM, Kuo YH, Lin TC, Horng TL, et al. Undular bore theory for the Gardner equation. *Phys Rev E*. 2012;86:036605. http://dx.doi.org/10.1103/ PhysRevE.86.036605.

- Environmental stratified flows. Edited by R. Grimshaw. Kluwer, 2001. J Fluid Mech. 2003;475:409–412. http://dx.doi.org/10.1017/S0022112002283378.
- Helfrich KR, Melville WK. Long nonlinear internal waves. Annu Rev Fluid Mech. 2006;38(1):395–425. http://dx.doi.org/10.1146/annurev.fluid.38.050304.092129.
- Ruderman M, Talipova T, Pelinovsky E. Dynamics of modulationally unstable ion-acoustic wavepackets in plasmas with negative ions. J Plasma Phys. 2008;74:639–656.
- Watanabe S. Ion acoustic soliton in plasma with negative ion. J Phys Soc Japan. 1984;53(3):950–956. http://dx.doi.org/10.1143/JPSJ.53.950.
- Rahman MM, Alam MS, Mamun A. Positron-acoustic gardner solitons and double layers in electron-positron-ion plasmas with nonthermal electrons and positrons. Eur Phys J Plus. 2014;129. http://dx.doi.org/10.1140/epjp/i2014-14084-4.
- Betchewe G, Victor KK, Thomas BB, Crepin KT. New solutions of the Gardner equation: analytical and numerical analysis of its dynamical understanding. *Appl Math Comput.* 2013;223:377–388.
- Kassam AK, Trefethen LN. Fourth-order time-stepping for stiff PDEs. SIAM J Sci Comput. 2002;26(4):1214–1233.

- Matthews PC, Cox SM. Exponential time differencing for stiff systems. J Comput Phys. 2002;176(2):430–455.
- 16. Higham NJ. Accuracy and Stability of Numerical Algorithms. SIAM; 1996.
- Friesner RA, Tuckerman LS, Dornblaser BC, Russo TV. A method for exponential propagation of large stiff nonlinear differential equations. J Sci Comput. 1989;4:327–354.
- Hepson OE, Korkmaz A, Dag I. Exponential B-spline collocation solutions to the Gardner equation. Int J Comput Math. 2020;97(4):837–850.
- Hamdi SA, Morse B, Halphen B, Schiesser W. Conservation laws and invariants of motion for nonlinear internal waves: Part II. Nat Hazards. 2011;57(3):609–616.
- motion for nonlinear internal waves: Part II. *Nat Hazaras*. 2011;57(3):609–616.

 20. Drazin PG, Johnson RS. *Soliton: An Introduction*. Cambridge University Press; 1989.
- Yousefi Y, Muminov KK. A Simple Classification of Solitons. Dushanbe: Academy of Science of Republic of Tajikistan; 2012.
- Schmelzer T. The Fast Evaluation of Matrix Functions for Exponential Integrators [Ph.D. thesis]. Oxford University; 2007.
- Schmelzer T, Trefethen LN. Evaluating matrix functions for exponential integrators via Carathéodory-fejér approximation and contour integrals. ETNA. Electron Trans Numer Anal. 2007;29:1–18. URL http://eudml.org/doc/117658.